

Original citation:

Mohamed, Ikhsan, Hutchins, David A., Davis, Lee A. J., Laureti, Stefano and Ricci, Marco .
(2016) Ultrasonic NDE of thick polyurethane flexible riser stiffener material. Nondestructive Testing and Evaluation . pp. 1-20.

Permanent WRAP URL:

<http://wrap.warwick.ac.uk/81819>

Copyright and reuse:

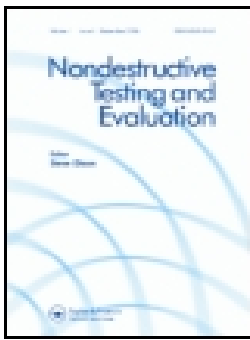
The Warwick Research Archive Portal (WRAP) makes this work of researchers of the University of Warwick available open access under the following conditions.

This article is made available under the Creative Commons Attribution 4.0 International license (CC BY 4.0) and may be reused according to the conditions of the license. For more details see: <http://creativecommons.org/licenses/by/4.0/>

A note on versions:

The version presented in WRAP is the published version, or, version of record, and may be cited as it appears here.

For more information, please contact the WRAP Team at: wrap@warwick.ac.uk



Ultrasonic NDE of thick polyurethane flexible riser stiffener material

Ikhsan Mohamed, David Hutchins, Lee Davis, Stefano Laureti & Marco Ricci

To cite this article: Ikhsan Mohamed, David Hutchins, Lee Davis, Stefano Laureti & Marco Ricci (2016): Ultrasonic NDE of thick polyurethane flexible riser stiffener material, Nondestructive Testing and Evaluation, DOI: [10.1080/10589759.2016.1241253](https://doi.org/10.1080/10589759.2016.1241253)

To link to this article: <http://dx.doi.org/10.1080/10589759.2016.1241253>



© 2016 The Author(s). Published by Informa UK Limited, trading as Taylor & Francis Group



Published online: 17 Oct 2016.



Submit your article to this journal [↗](#)



Article views: 100



View related articles [↗](#)



View Crossmark data [↗](#)



Ultrasonic NDE of thick polyurethane flexible riser stiffener material

Ikhsan Mohamed^a, David Hutchins^a, Lee Davis^a, Stefano Laureti^{a,b} and Marco Ricci^b

^aSchool of Engineering, University of Warwick, Coventry, UK; ^bDipartimento di Ingegneria, Università degli Studi di Perugia, Terni, Italy

ABSTRACT

Ultrasonic signals at frequencies below 1 MHz have been used for the NDE of thick polymer samples. Coded signals such as chirps and bipolar Golay codes, together with pulse compression and signal processing, have been used to penetrate into thick sections of attenuating polypropylene riser stiffener material, using piezocomposite transducers to provide the required bandwidth. It is shown that this approach can be used to detect manufacturing defects such as air bubbles in flexible riser stiffeners, which might compromise their performance in the offshore oil and gas environments.

ARTICLE HISTORY

Received 14 June 2016
Accepted 15 September 2016

KEYWORDS

Pulse compression; cross correlation; piezocomposite; polyurethane; SAFT

1. Introduction

In performing NDE of large industrial infrastructure, problems can arise due to poor signal to noise ratios (SNRs). This is especially the case when the materials involved are difficult to test because the ultrasonic signal is either attenuated or scattered, leading either to lack of signal due to attenuation, or to the presence of extremely high levels of scattering noise. Materials that could exhibit these properties are fibre reinforced composites, concrete and viscoelastic polymers. For these reasons, ultrasonic frequencies below 1 MHz are sometimes selected for use in highly attenuating and scattering materials, as the longer wavelengths and lower intrinsic attenuation can increase the depth of penetration into the sample. However, such lower frequencies will also reduce the resolution of the resulting image or measurement, because of the longer wavelengths. Signal processing has thus been investigated to try and alleviate these problems.[1] Other methods include modification of transducer shape, size, and frequency. The use of larger synthetic apertures (leading to the Synthetic Aperture Focusing Technique (SAFT) imaging approach [2,3]) has also been reported as a means of increasing resolution and SNR values.

Polyurethane has been used widely in many industries and is an important polymer due to its uses in manufacturing many different products. The properties of the polymer can be adjusted during manufacture to give a wide range of mechanical properties. For example, in the form of a foam it can be used for nonflexible, high-resilience foam seating; rigid foam

CONTACT David Hutchins  D.A.Hutchins@warwick.ac.uk

© 2016 The Author(s). Published by Informa UK Limited, trading as Taylor & Francis Group.

This is an Open Access article distributed under the terms of the Creative Commons Attribution License (<http://creativecommons.org/licenses/by/4.0/>), which permits unrestricted use, distribution, and reproduction in any medium, provided the original work is properly cited.

insulation panels and microcellular foam seals and gaskets. It can also be used in durable elastomeric wheels and tires (as used for escalator wheels), automotive suspension bushings, synthetic fibers and many other areas.[4,5] Because of its special properties such as high load capability, flexibility, tear resistance and resistance to water, it has been used in the oil and gas industry for many years. Of particular interest here is its use specifically in the sea bed oil logging, as part of a flexible riser system [6] or as a bend stiffener [7]. The flexible riser allows the oil platforms to move with wind and tides etc., while remaining connected to the sea bed. Riser or bend stiffeners are used to restrict the motion of the riser, so as to avoid catastrophic failure due to fatigue or excessive motion of the riser at the connection point. The stiffener often has a hollow conical shape, with additional steel components to allow the riser and stiffener to be connected together. Obviously, following oil spills in highly-fragile ecosystems in recent years, it is very important that the structural integrity of such structures can be maintained in such a complicated and hostile environment.[8–11]

Measurement of the ultrasonic properties of polyurethane in bulk solid form has only received limited study, and usually in thin samples. For example, it has been studied by ultrasound when used for the strengthening of composite structures.[12] As a foam product, air-coupled ultrasonic techniques can be used, due to the low acoustic impedance of the material which is better-matched to air than many materials.[13] The use of polyurethane paint coatings has also been observed to affect laser-based ultrasonic NDE systems.[14] However, the NDE of large bulk polyurethane material, as used in bend stiffeners, seems not to have been described in the literature. As will be shown in this paper, polyurethane riser stiffener material is extremely attenuating of ultrasound at frequencies above 1 MHz, where conventional ultrasonic NDE typically operates. However, it is difficult to construct conventional piezoelectric transducers with wide bandwidths at lower frequencies, although, as will be shown below, piezocomposites show promise in this regard. It is thus important to design the excitation and processing methods to utilise the available bandwidth to maximum effect, optimising the SNR and hence depth of penetration into the material, while also allowing imaging of defects.

In this paper, Pulse Compression (PuC) techniques will be used at frequencies in the 100–500 kHz range to obtain information about difficult materials or structures, using piezocomposite transducers to extend the available bandwidth. Such a combination has been seen to give good results. PuC relies on a matched-filter approach, where a long-duration excitation waveform is used across the available bandwidth.[13,14] It is thus possible to overcome the problem of peak-power limitation using a lower voltage but longer time-duration signal, and then to process this signal so that spatial resolution and SNR are optimised. PuC techniques traditionally involve the transmission of a long coded pulse and the processing of the received signal to compress the output into a much shorter temporal signal: this compression is achieved by cross-correlating the output and the input signals.[15] PuC can be thus used in principle on more highly attenuation materials and to detect smaller flaws at longer distances than are possible with conventional pulsed NDT systems.

There are many types of waveform that can be used for PuC. The problem to be overcome at low frequencies is that there will be a limited bandwidth available, making the choice an important consideration. Thus, for example, a narrow bandwidth piezoelectric transducer may use a different waveform to one based on wider-bandwidth piezocomposites. Waveforms such as linear FM chirps, random noise and Golay binary codes have all been investigated in ultrasonic testing,[16,17] and each have their own properties. In this paper,

two types of signal will be compared for use at low frequencies, namely a linear FM signal (Chirp) and a bipolar Golay binary coded waveform. Note that Golay codes are available in both conventional and bipolar form – the latter is chosen here because it is able to deal more effectively with transducers with a specific centre frequency.[18] Such codes have found use in biomedical imaging systems, for example [19–21].

As will be shown, PuC data was collected in a way that lends itself to both standard C-scan imaging and SAFT imaging.[2] A typical SAFT algorithm consists of the time-of-flight corrected superposition of the recorded signal. It has been shown that SAFT can lead to up to 20 dB SNR gain in ultrasonic testing applications.[3] Thus, defects which are undetectable with standard ultrasonic imaging could be highlighted if SAFT is used for the coherent reconstruction of ultrasonic images.

2. Apparatus and method

Figure 1(a) shows the sample chosen for this study. This was a polyurethane section, which was part of a larger structure used within a riser stiffener in the underwater oil and gas industries. The sample shown was 1.2 m long, and 0.16 m thick at its thicker end. The material was found to be sufficiently attenuating that conventional signals at frequencies >1 MHz could not be used for the imaging of defects. A PuC system was thus designed, based on a pair of piezocomposite transducers with a centre frequency of 300 kHz. The transducers were 25.4 mm in diameter. Figure 1(b) shows a pair of these devices for use in pitch-catch mode. The transducers were fitted with a matching layer for water – this gave reasonable transmission efficiencies into the polyurethane sample, whose acoustic impedance was much lower than that of typical metal samples, for example. A pitch-catch configuration was used, as pulse-echo measurements were not very practical with a PuC system. This is because the long duration of the excitation waveforms overloaded the receiver electronics for a sufficiently-long time that near surface defects would be missed. Measurements could also be taken in through-transmission, as in Figure 1(a), so as to measure the attenuation properties of the material, or in pitch-catch for imaging purposes.

The waveforms (either chirp or binary) were generated using an arbitrary waveform generator within a National Instruments PXI system, and the centre frequency (f_0) of the drive signal adjusted to suit the maximum response of the piezocomposite transducers. The PXI system had a maximum output voltage of 15 V, but typically only 4 V was needed

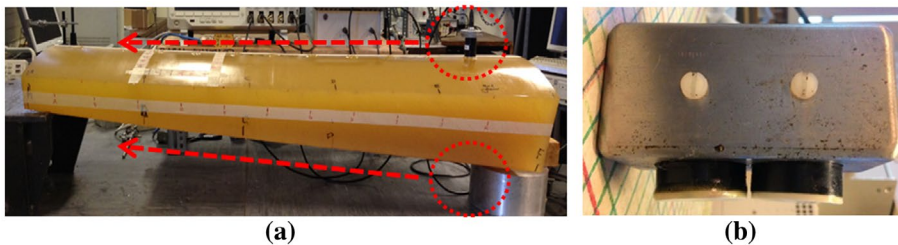


Figure 1. (a) A through transmission ultrasonic measurement of the thick polyurethane sample using two piezocomposite probes (locations identified by the red dashed circles); these could scanned in unison along the sample in the direction of the arrow. (b) A pair of spring-loaded piezocomposite transducers devices used for single-sided pitch-catch measurements.

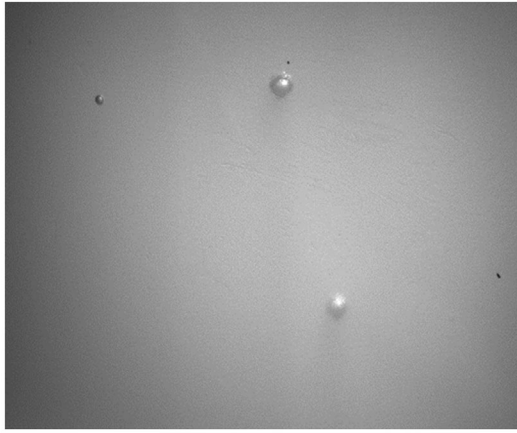


Figure 2. Optical image of the bubble defects in the polyurethane riser stiffener samples. The bubbles were approximately 5–7 mm in diameter, and of unknown depth into the sample.

to drive the transmitter for the measurements reported here, although a voltage amplifier could be inserted if needed. The receiving transducer was connected to the receiver section of the PXI system, and digitised before being processed for PuC.

The sample contained natural defects which were formed during manufacture, these being air bubbles of different sizes and depths within the sample. Figure 2 shows an image, obtained using an optical imaging system in through-transmission through the sample, of two such defects, at a region where the sample was 100 mm thick. This shows two bubbles of ~5–7 mm diameter, where the lower bubble in the image is deeper into the material, noting that this depth was difficult to estimate visually (and noting that this method would not be feasible for a real in-service NDE inspection). In addition, a 10 mm diameter hole was drilled manually into the lower surface of the sample, at a different location to simulate the presence of a defect of known dimensions. This hole was drilled to a depth of 70 mm from the bottom surface of the sample at a region where the sample thickness was 150 mm (i.e. the bottom of the hole was 80 mm from the top surface). The transducers were placed as in Figure 1(b) for imaging in the pitch-catch configuration. Data was collected on a grid of 23 (*X*-direction) by 35 (*Y*-direction) acquisition points for imaging purposes. This was achieved by scanning an area of 46 mm by 70 mm, with the probes moved in unison in their holder (Figure 1(b)) in steps of 2 mm. A PuC waveform was recorded at each position. The spring loading of the transducers onto the surface helped to maintain a reasonably constant coupling force onto the sample, using conventional NDE ultrasonic coupling gel.

A simulation was performed to establish the combined directional characteristics and sensitivity of the pair of transducers shown in Figure 1(b), an important characteristic for imaging systems.[22] If d and λ are the transducer diameter and the ultrasonic wavelength in the material, the near-field distance limit Z can then be calculated from Equation (1):

$$Z = \frac{d^2}{4 * \lambda} \quad (1)$$

The longitudinal velocity in the polyurethane sample was 1700 ms^{-1} , and the centre frequency of the excitation waveform was 300 kHz, using piezocomposite transducers of

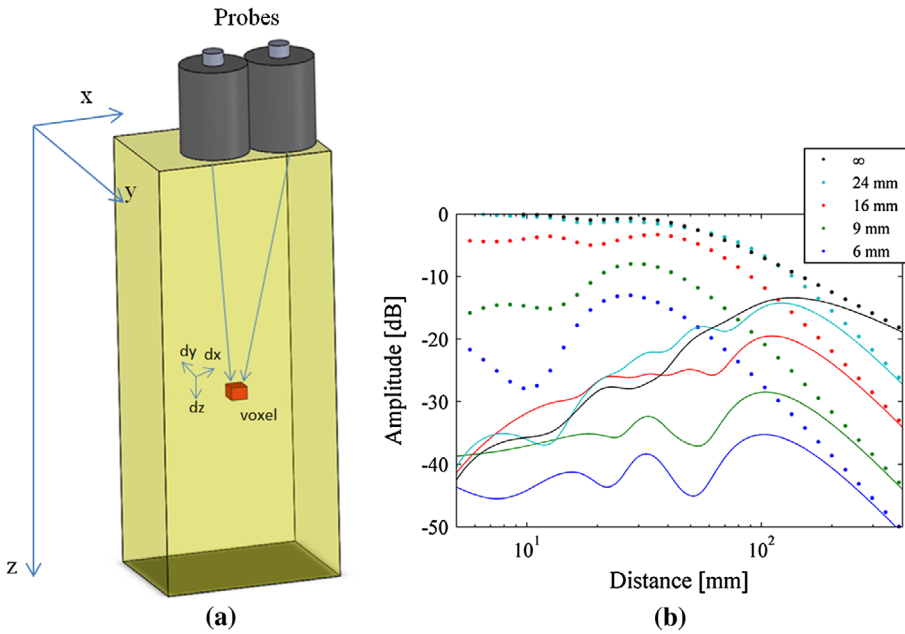


Figure 3. (a) Geometry for simulating the transducer response in pitch-catch mode. (b) Simulated DGS at 350 kHz, for different defects sizes, assuming transducers of 25.4 mm diameter and a polyurethane sample. Solid lines: a pitch-catch transducer pair; dashed lines: a single transducer in pulse-echo. The coloured lines show the expected received amplitude levels for spherical defects whose diameter is 24, 16, 9 and 6 mm respectively. Also shown is the response for a defect of infinite width.

27 mm diameter. Thus, we obtain $Z = 32$ mm. This value is valid only if a single transducer is considered. Further investigation was needed if two transducers in pitch-catch configuration were to be used for the signal generation/acquisition, as in this work, where both transducers operate at normal incidence, but with overlapping beam profiles within the sample. Thus, a series of numerical simulations was performed, using the geometry shown in Figure 3(a). The approach followed is similar to that used for Distance Gain Size (DGS) diagrams.[23] DGS diagrams are designed to show the variation of echo amplitude with range and target size. Here, the expected defect signal amplitude is calculated with respect to the back-wall echo, which is considered as a perfect reflector. The simulated DGS curve at 300 kHz for either a single transducer in pulse-echo mode (continuous lines) or a pair of transducers in pitch-catch mode are shown in Figure 3(b). The black line (either in foreground or in background) shows the expected signal amplitude from a perfect reflector. In the near field (at smaller axial distances), the simulations show that a pulse-echo arrangement (background blurred lines) is significantly more advantageous than a pitch-catch geometry (foreground) for geometrical reasons – the transmitted and received beams overlap more effectively. However, in the far-field, the pitch-catch sensitivity is similar that for pulse-echo. The SNR gain of PuC then improves signal detectability. This is an important feature if signals are to be retrieved from very lossy materials at large distances.

In order to understand better the 3D sensitivity field behaviour of the two probes, a series of numerical simulations have been carried out. The Rayleigh-Sommerfeld integral model has been used for these simulations, together with the piston-transducer approximation.[24]

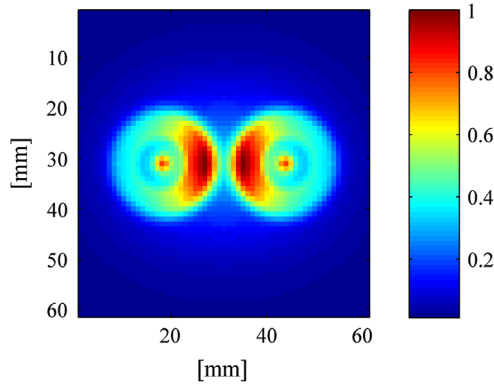


Figure 4. Simulated sensitivity for the pair of piezocomposite transducers at 300 kHz, at a depth of 5 mm into the sample.

This allows the spatial distribution of the transmitter and detector fields to be determined at a particular frequency, and hence the sensitivity of the transducers to a certain location in 3D space to be determined. As an example, simulation results are shown in Figure 4 for operation at a depth of 5 mm into a polyurethane sample, where the combined sensitivity level of the two probes has been plotted at 300 kHz. It can be seen that sensitivity is greatest in the regions along a line joining their two centres, as might be expected.

Because of the directionality shown in Figure 4, it would be expected that alignment of the pair on the surface of the sample relative to a scan direction across the surface would have an effect. To illustrate this, Figure 5 shows the spatial variations in 3D transmit/receive sensitivity for a pitch-catch pair at a certain location on the sample (noting that the transducer pair would be scanned along the top surface at the fixed distance apart in the direction shown by the red arrow. It can be seen that the probe sensitivity is not uniform in regions close to the surface, where the beams from the two transducers have not overlapped fully. This is of importance, especially if a small defect is to be detected at a small depth from the scanning surface, as the detectability would be a function of the transducer pair orientation. However, it can also be seen that this effect becomes less marked with depth into the sample, so that at a depth of ~ 100 mm, the spatial response is relatively well-behaved, with a maximum on-axis and a decreasing sensitivity with increased radial distance. In the sample being studied, the flat-bottomed hole defect is within the near-field region, and hence far-field behaviour cannot be assumed. Note also that this far-field condition is reached at a distance which is several times greater than the nominal near-field limit expected for a single transducer (32 mm, as calculated from Equation (1)).

3. Results and discussion

3.1. Attenuation coefficient of the polyurethane material

The first experiment determined the attenuation properties of the material, and was set up as shown earlier in Figure 1(a). A chirp was used as the input signal, noting that the range of frequencies ($f_2 - f_1$) covered by the chirp can be adjusted, as can the total time duration (T) and the centre frequency (f_0). In this case the values were $T = 0.07$ ms, $f_2 - f_1 = 250$ kHz and

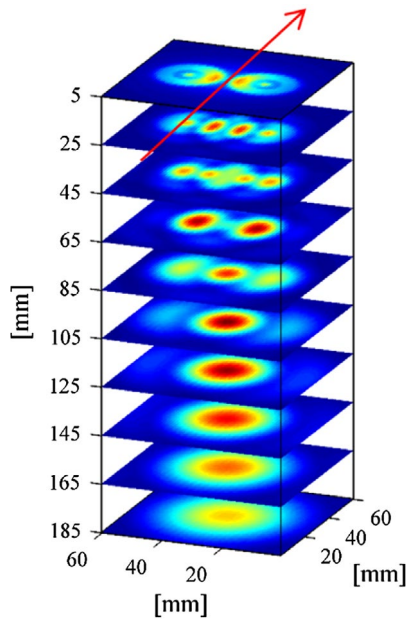


Figure 5. Simulated 3D sensitivity field for two piezocomposite transducers in pitch-catch mode. The red arrow shows a scan direction perpendicular to the line joining the transducer centres, as calculated from Equation (1).

$f_0 = 275$ kHz. In this experiment, two piezocomposite probes were used as the transmitter and receiver in a through-transmission arrangement, where one of the probes was placed on top of the sample and the other probe held by hand below the sample. Measurements were taken at 10 cm intervals along the length of the sample, the thickness varying from 8.8 to 15 cm. At every point, measurements were repeated 10 times and all waveforms recorded. Data was processed using Matlab, where the peak amplitude and frequency were recorded. A graph of amplitude (in dB) vs. thickness was plotted, as shown in Figure 6. Here, the slope of the graph gave the attenuation coefficient of the Polyurethane sample, which was estimated to be ~ 1 dB/cm at 300 kHz. Note that the present results have not been corrected for diffraction effects, and hence do not consider the transducer characteristics explicitly. However, they do give an indication of the level of signal loss in the polyurethane material.

3.2. Choice of PuC scheme

The coded waveform has to be chosen carefully, so that it produces the maximum output from a given transducer. In the experiments, two types of signal were compared for use at low frequencies, namely a linear FM signal (Chirp) and an Inverse Repeated Sequences Golay (IRS-Golay) binary coded waveform.[25] Note that traditional Golay-code system would be expected to be better-suited to wide bandwidth transduction systems, whereas the chirp could be tuned to suit a narrower, more resonant transduction system to maximum effect. In the present case the transducers have a quite large bandwidth, so both schemes could work. In particular, the IRS Golay scheme allows a centre frequency to be selected, so it was preferred with respect to the standard one.

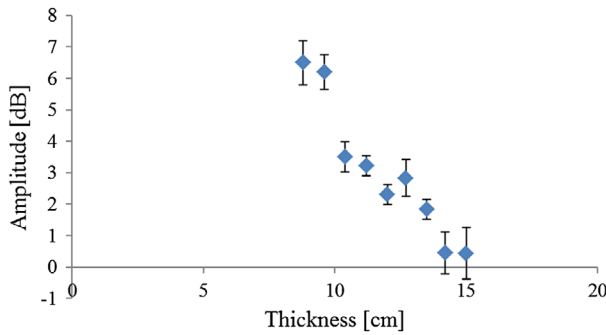


Figure 6. Graph of received amplitude (dB) vs. thickness at a frequency of 300 kHz for the polyurethane material.

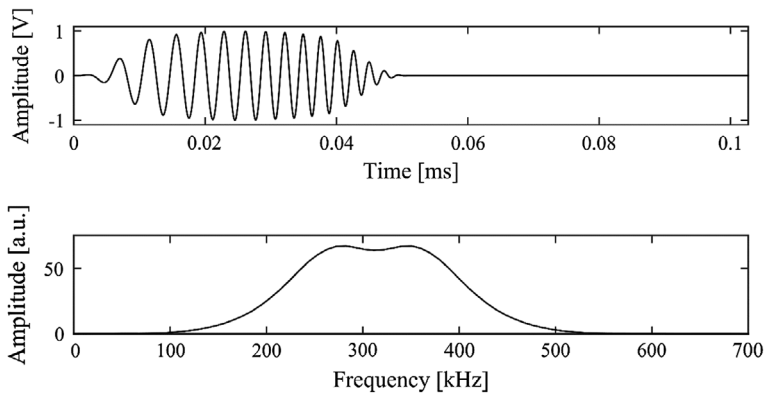


Figure 7. Voltage drive Chirp signal, and its spectrum obtained using an FFT.

Figures 7 and 8 show both the chirp and IRS-Golay signals that were used in a comparative test, using the same drive voltage level of 2 V pk – pk. It can be seen that the linear chirp was windowed so as to have a smooth transition in the power spectrum density, using an Elliptical-Tukey window.[26] This ensured that the autocorrelation of the chirp signal had a low level of side lobes.

It can also be seen from the FFT (Figure 8) that the bandwidth of the IRS-Golay was greater, and extended almost to DC even if it does not have a completely symmetrical frequency spectrum. In addition, the spectrum amplitude of the bipolar Golay code was higher than that of the chirp. This is because the bipolar Golay uses a pair of waveforms to obtain its characteristics, each one having twice the power of the chirp signal so that, fixed the duration of the single waveform, the Golay energy is four times that of the windowed chirp energy.[19,25] Note that for the sake of figure clarity in Figures 7 and 8 short signals were depicted, while the experimental data (see Figures 10 and 11) were collected by using a thirty-time longer Chirp of about 1.5 ms to increase the SNR gain and the compression quality, as explained afterwards.

Figure 9 shows the autocorrelation output of chirp and bipolar Golay signals (i.e. after they have been cross-correlated with themselves).

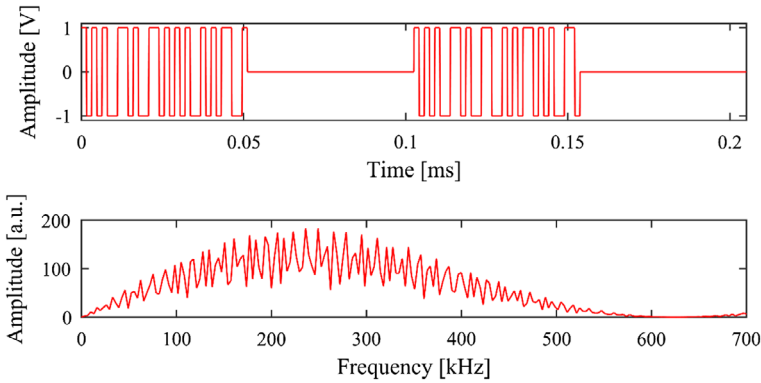


Figure 8. Voltage drive bipolar Golay signal, and its spectrum obtained using an FFT.

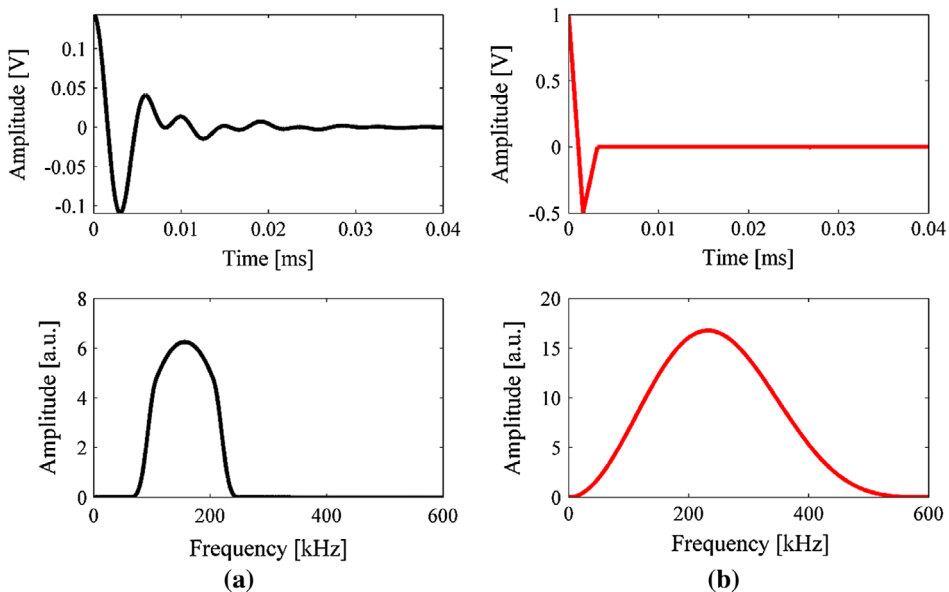


Figure 9. Autocorrelation outputs of (a) Chirp and (b) bipolar Golay code signals, showing the time waveform at the top and the corresponding frequency spectrum below.

Figure 10 shows the result of a pitch-catch experiment, in which signals were reflected from one of the air-bubble defects of Figure 2, located approximately at 50 mm below the sample surface. The two figures show the differences in the response when either the chirp or the Golay code was used with the pair of broad bandwidth piezocomposites. For chirp excitation, it is clear that a very good signal was obtained with the piezocomposite pair, showing that PuC had worked very well with these transducers in this highly-attenuating material. In particular, the extension of bandwidth up to frequencies of 350 kHz was an excellent result. For the Golay code excitation, this bandwidth was extended even further.

In practice, a chirp with a 312 kHz centre frequency, a 300 kHz bandwidth and a total time duration of 1.5 ms was found to be an excellent waveform to use – while the IRS-Golay had a more extended bandwidth, it was found more convenient to tailor the frequency

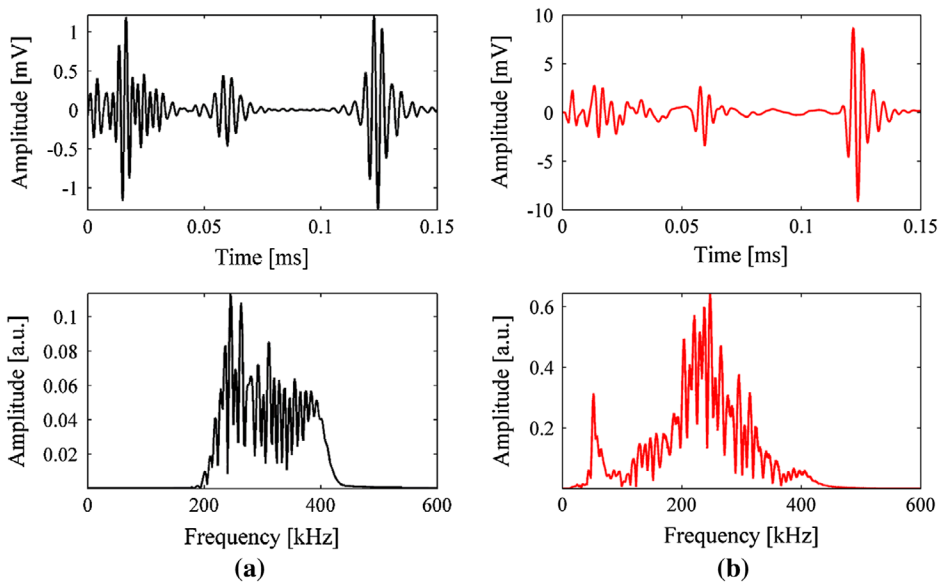


Figure 10. Detection of a sub-surface defect using PuC and (a) a chirp and (b) bipolar Golay-Code excitation for a pair of wide bandwidth piezocomposite transducers.

range of the chirp to get maximum output from the piezocomposites – important in lossy materials. Also, Elliptical-Tukey windowing allowed the influence of side-lobes in the frequency response to be reduced. It was found that this optimised the amount of energy that was utilised by the transducers. In addition, as safety rules need to be taken into account for on-site inspection of off-shore oil and gas structures. Hence, the signal voltage used to the transmitter was only 1 V. A Cooknell charger amplifier was used to enhance the received signal level.

An example of the received signal, both before and after pulse-compression, is shown in Figure 11. This demonstrates not only that a small bubble defect could be detected, but that a clear signal from the back-wall was also present, illustrating the excellent penetration of the signal into the polyurethane riser stiffener material.

3.3. Imaging of defects within the polyurethane sample

3.3.1. Defects and imaging methods

Two types of defects were examined. The first type was artificial defects in the form of flat-bottomed holes, machined into the bottom surface of the sample. These were of known size, shape and location, and allowed the imaging algorithms to be tested fully. The imaging methods were then used on the air bubble defects created during manufacture, examples of which were shown earlier in Figure 2. A set of measurements were collected over a grid of 23×35 points, with a grid resolution of $2 \text{ mm} \times 2 \text{ mm}$. The raw data was acquired at each scanning point (x, y) and stored in a 3D matrix.

Two types of imaging were performed. The first was a standard C-scan approach, whereby the data could be displayed as horizontal sections of the material, or extrapolated into a B-scan (effectively a vertical section). The second approach was SAFT imaging.[2] It has

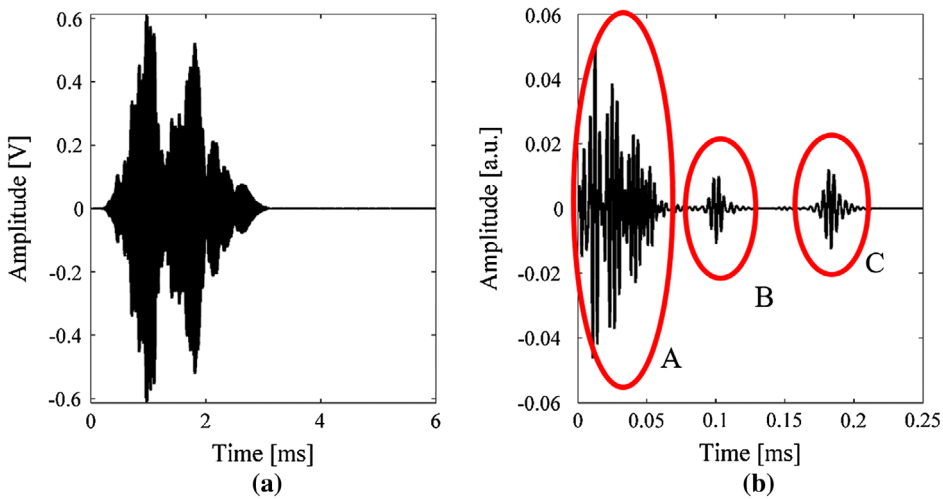


Figure 11. Results after PuC from an experiment using a windowed chirp excitation signal in a polyurethane sample of 150 mm thickness and for a 6 mm diameter defect at a depth of 70 mm. (a) the received time signal before cross-correlation, and (b) the PuC output. In (b), region A is due to electrical cross-coupling, B is the defect echo, and C is the reflection from the back wall.

been shown that SAFT can lead to up to 20 dB SNR gain in several ultrasonic testing applications.[3] Thus, defects which are undetectable with standard ultrasonic imaging could be highlighted if SAFT is used for the coherent reconstruction of ultrasonic images, and was thus of interest here. Moreover, SAFT increases spatial resolution of the reconstructed images allowing a better evaluation of the size of a defect [27]; in addition, the final image resolution can be varied. A control volume (mesh) made up of a defined number of voxels (3D pixels) was constructed, as was shown earlier in Figure 3(a). The dimensions of each voxel in the control volume could be tailored to obtain a good trade-off between reconstruction computational time and image quality. In general, SAFT assumes the far-field condition and coherently sums the received signals by applying a mathematical weight to them, derived from the far-field assumption. However, in the present case both the drilled hole and the air bubbles were within the near-field zone. Thus, the 3D simulated field shown in Figure 5 was used to weight the response from each location. This helped to reduce noise levels in the images.[28]

3.3.2. Detection and characterization of flat bottom hole defect

The aim of this test was to examine the ability of the system to detect features of known defects such as the location, shape and size. For this purpose, a flat-bottomed hole was machined into the sample using 10 mm drill bits. This hole was drilled to a depth of 7 cm from the bottom surface of the sample at a region where the sample thickness was 15 cm (i.e. the bottom of the hole was 8 cm from the top surface). Different visualizations of the C-scan data are shown in Figure 12. The 3D view shows the presence of the defect (top part of the drilled hole) at a depth of 8 cm from the top surface. However, it can also be seen that the part of the image closest to the surface contains a cross-coupling signal between the two probes. Although this signal can be reduced by exploiting several different post-processing techniques,[3] it cannot be totally avoided. As expected, the back-wall echo appears at a

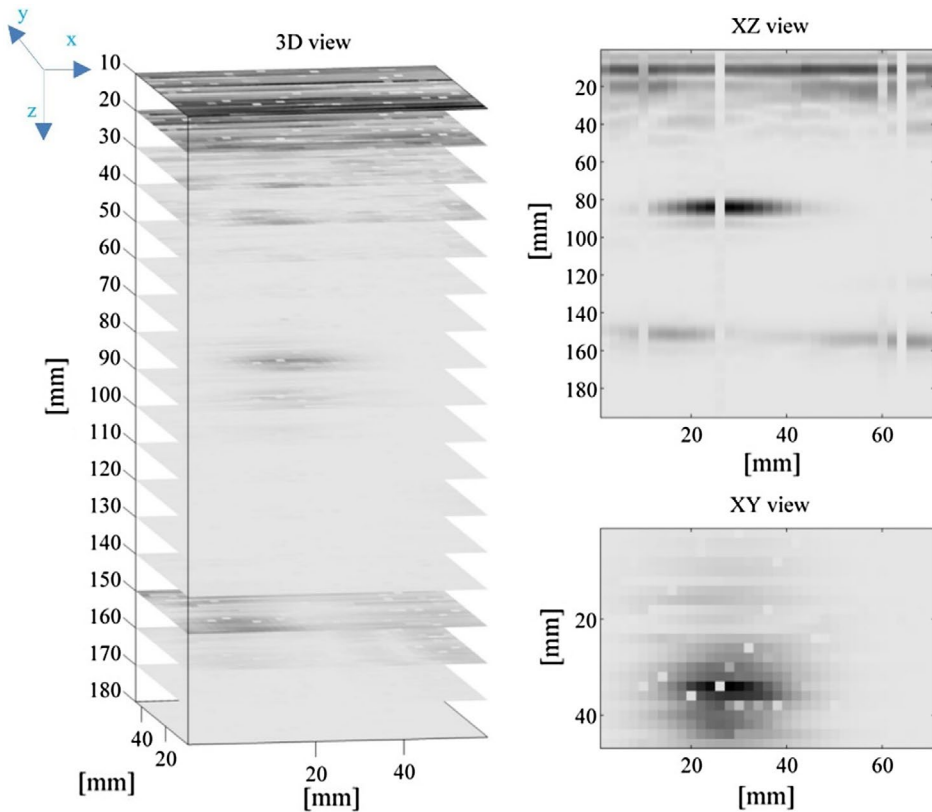


Figure 12. C-Scan results for the artificial defect in the form of a flat-bottomed hole.

depth of 15 cm. The reconstructed B-scan (XZ view) shows clearly the presence of the hole. The blurred defect shape is mainly due to the dimension of the probes and the frequency range (relatively low) used for this imaging test. Although the dimensions of the imaged defect are bigger than the real one, useful information such as defect depth and sample shape (see back-wall echo) can be extract from this view. The C-scan (XY view) shows the defect location relatively to the scanning area.

Consider now the SAFT image, which is shown in Figure 13. The results shows that the defect imprint is significantly enhanced and de-blurred with respect to a normal C-Scan image reconstruction. Moreover, the cross-coupling time duration is slightly diminished and the presence of defect signatures in the first 4 cm appear. Thus, the blind zone just beneath the transducer was estimated to have halved, from 40 to 20 mm. In this image, a voxel volume of $2 \times 2 \times 1$ mm was used for the dx , dy and dz dimensions respectively. This was found to be the optimum voxel volume. In real industrial applications, it is of utmost importance to realize an experimental setup which provides significant results without being slow. This can be achieved by lowering the computational constraints, for example by lowering the number of (x, y) experimental measurements taken into account for the algorithm. Figure 14 shows the results obtained for sub-sampling the measurement grid by a factor of two. As can be seen, the image is slightly degraded, but not markedly. This demonstrates that at these low frequencies, data need not be collected at too fine a spatial interval on the surface.

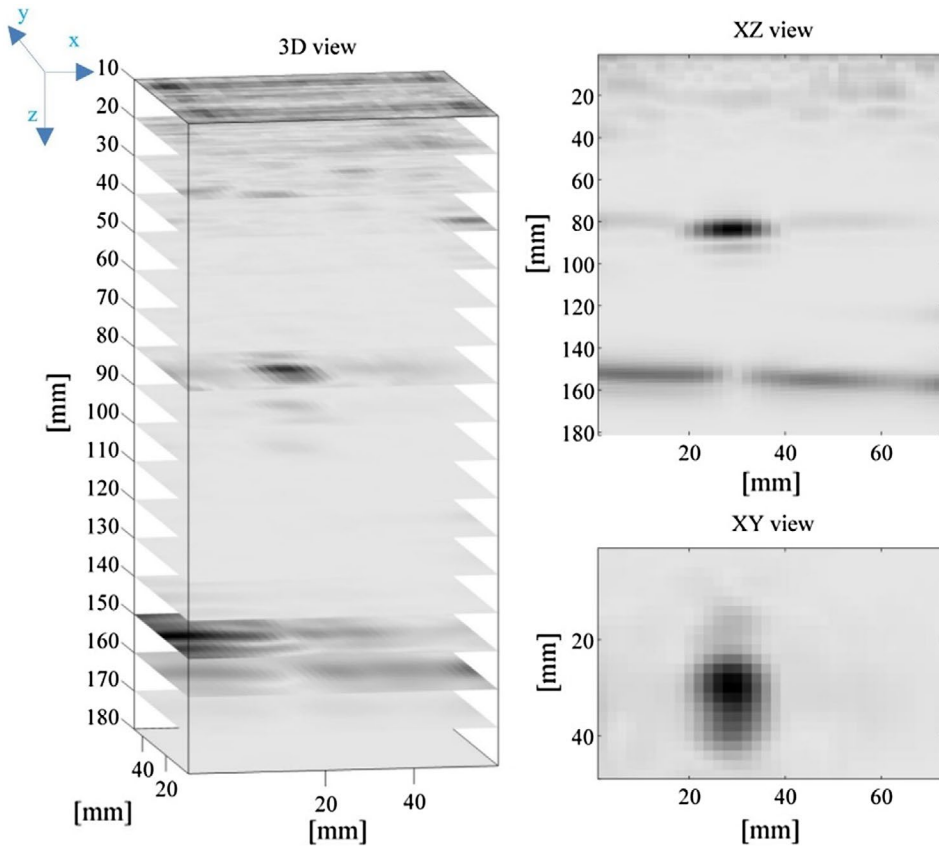


Figure 13. SAFT results for the same data-set as the C-scan of Figure 9.

3.3.3. Detection and characterization of air bubble defects

The collected data were processed using MATLAB. The defect echoes were identified and their peak-to-peak amplitude plotted in a matrix which represents the condition of the scanned area of the polyurethane sample. The image obtained from C-scan data is shown in Figure 15(a), where it is clear that the two defects were detected within the scan area. A typical PuC output over a defect is shown in Figure 15(b). The C-scan indicates that the detected defect areas were similar in both cases, and the depth of each defect can be estimated as between 6–8 and 7–9 cm respectively. The darker area close to the surface is due to factors such as electrical cross-coupling between transmitter and receiver, and the presence of surface waves that travel between the two transducers.

To improve the image further, post processing techniques have been tested both during and after the application of PuC. In contrast to the standard PuC algorithm, where the data recorded by the transducers is cross-correlated with the time replica of the input signal (labelled ‘Standard’ in Figure 16(a)), the data could also be cross-correlated with the time replica of the signal recorded from either the direct contact of the two transducers (labelled ‘Probe’ or from a through-transmission measurement on a clean area of the sample (‘Material’). This allows a more realistic input of transducer and material properties into the reconstruction. It is observed that in the ‘Probe’ and ‘Material’ cases, the time duration

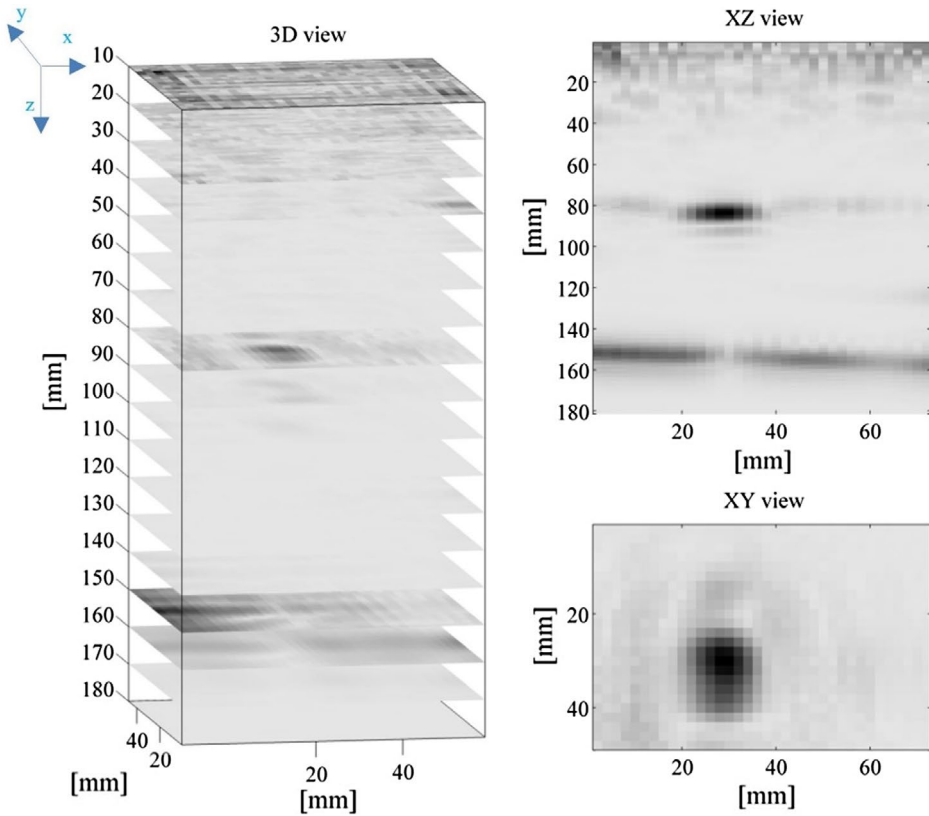


Figure 14. SAFT result using a sub-sampled data-set containing only half of the scan location (transducers data sampled at 4 mm spatial intervals on the sample surface).

of the cross-correlation peak reduces, leading to a better assessment of defect depth. Note that the amplitude is arbitrary and the red signal is the larger of the two. This illustrates clearly that the influence of the electrical coupling has been reduced. As alternative strategy to reduce both the noise close to sample surface and to improve depth resolution, a Total Variation (TV) deconvolution approach [29,30] has been applied to the ‘Standard’ case, see Figure 16(b).

The TV algorithm is able to enhance the imaging and inspection capability. This is demonstrated in Figure 17 by the 3D images obtained using these two different techniques, where the image intensities were normalized to the maximum intensity of the defect area, i.e. the bubble on the right side.

The SAFT approach detailed above for the flat-bottomed hole was also implemented, and the results are shown in Figure 18. In Figure 18(a), the data is shown first with the back-wall echo included as a linear scale of amplitude. The defects are not clearly visible in this visualization. However, by turning to a plot in dB (Figure 18(b)), the defects are now more evident. This is further improved if the back-wall echo is removed from the data (Figure 18(c)) by widening it out from the time-domain data.

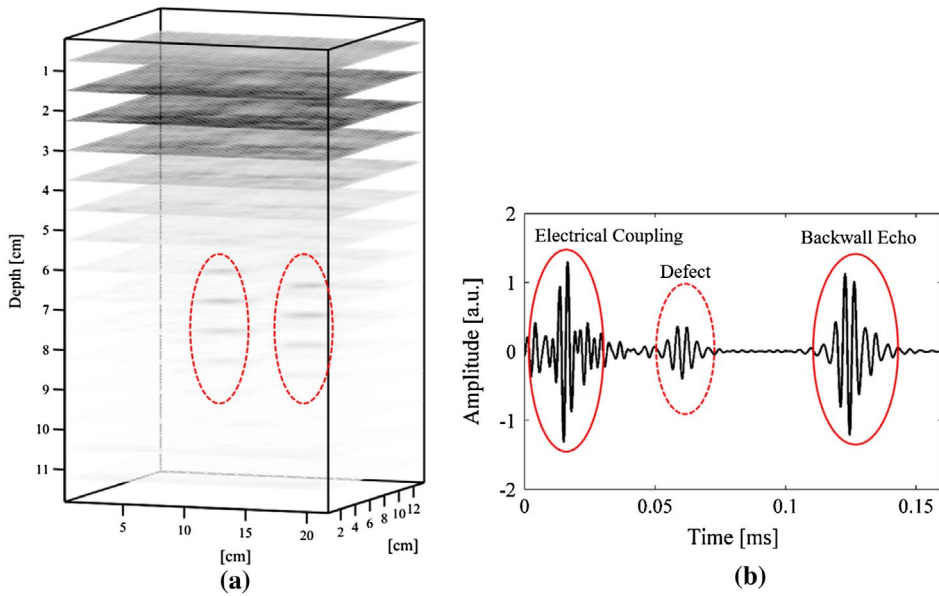


Figure 15. (a) 3-Dimensional imaging of the polyurethane sample. The two red ellipses that appear at depths of 6–9 cm indicate the location of the defects. (b) Typical PuC output in the form of an impulse response acquired from the polyurethane sample in the presence of a defect.

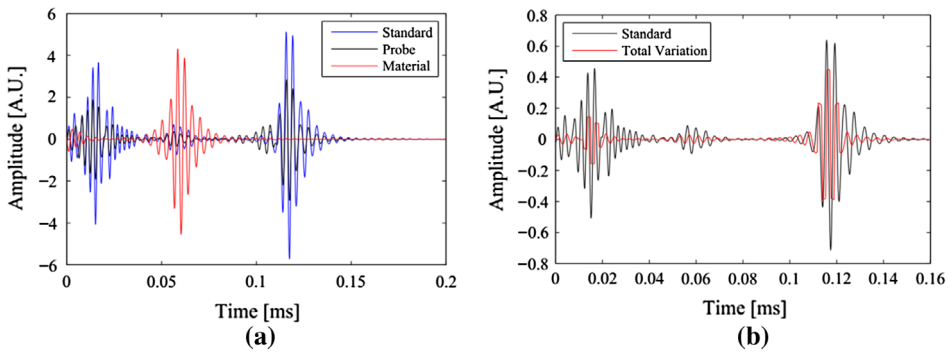


Figure 16. (a) Comparison between the standard matched filter technique (blue), the cross-correlation with the signal modified by the transducers spectrum (black) and by the sample + material properties (red); (b) Comparison between the standard matched filter technique (dark) and the Total Variation deconvolution (red).

3.3.4. Comparison between standard C-scan and SAFT image resolution

The results achieved by plotting a C-scan image after PuC have been compared to those obtained using the SAFT algorithm. Figures 19 and 20 show the C-scan obtained for both the above mentioned techniques together with two 1D sections of the C-scan along x and y directions. Please note that in the following figures a normalized dB scale was used with the same axis limits, so as to better appreciate the difference in the spatial resolution.

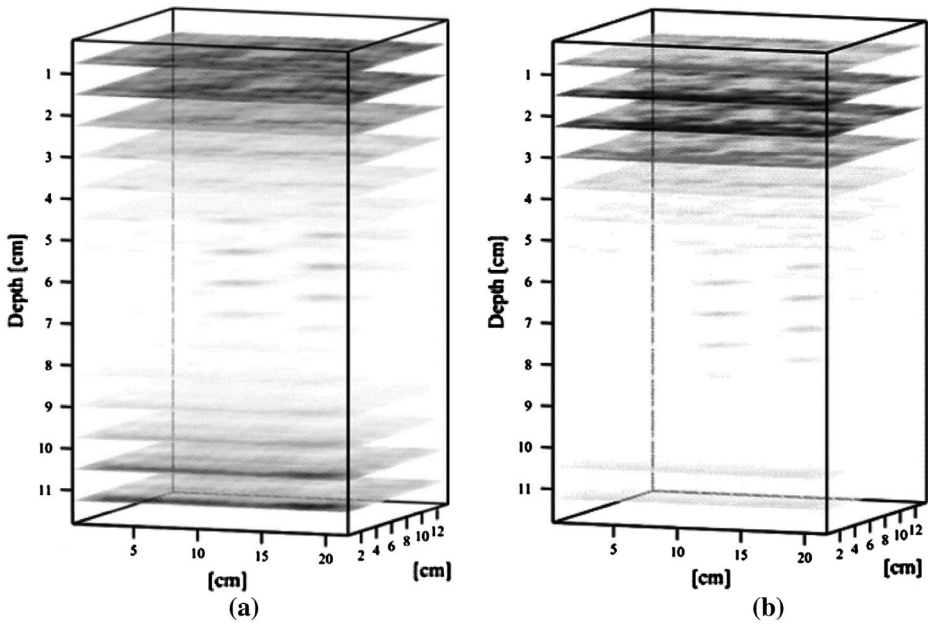


Figure 17. Three-Dimensional imaging obtained with the ‘Transducer’ recorded signal as (a) a matched filter and (b) with the Total Variation (TV) method.

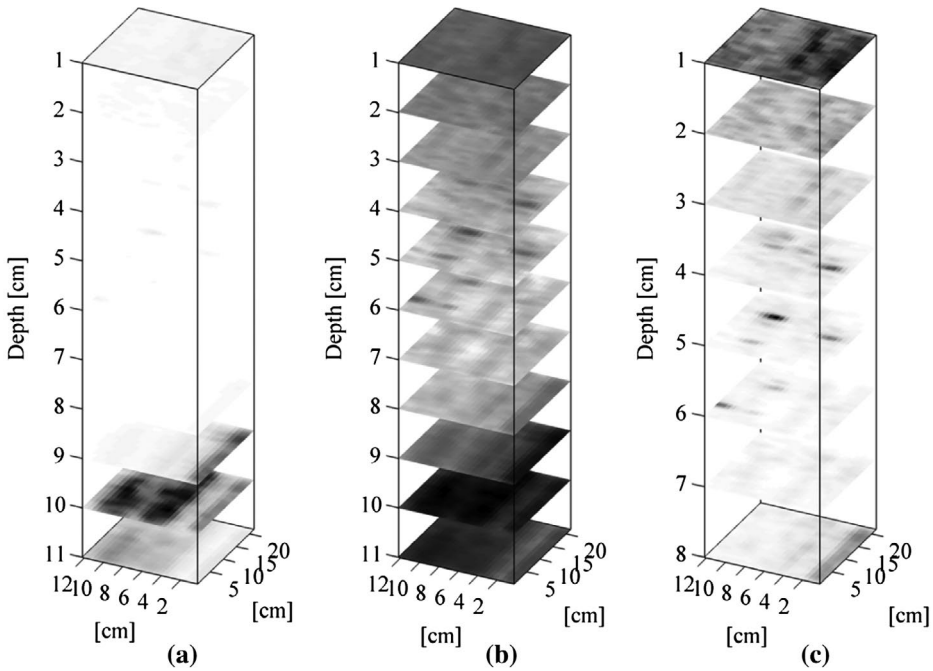


Figure 18. SAFT images of the hole defects shown in Figure 2. (a) Image plotted on a linear scale with the back wall echo data included; (b) as (a) but plotted with a dB scale; (c) as (a), but with the back wall echo excluded.

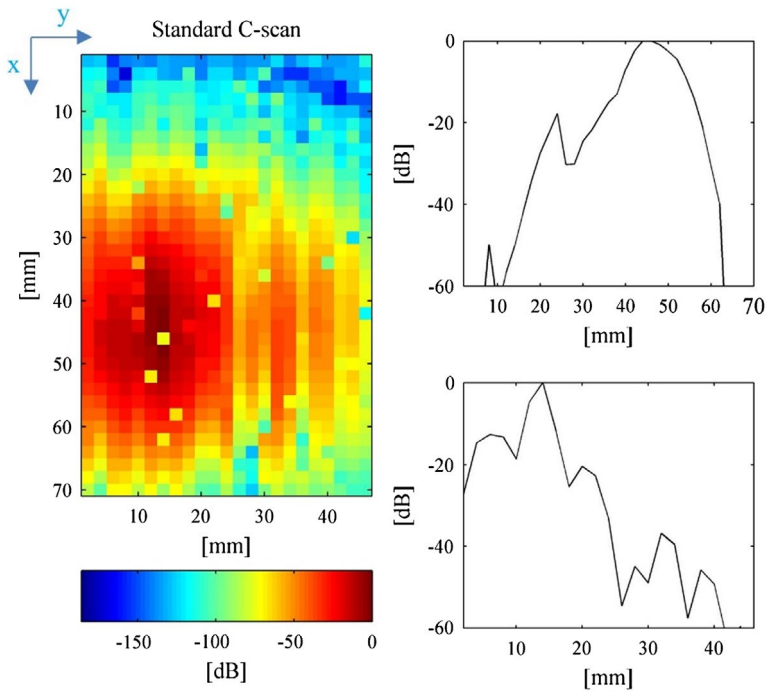


Figure 19. Analysis of the spatial resolution on raw data. (left) C-scan at $z = 80$ mm, (top right) cross-section of the C-scan along the x axis, (bottom right) cross-section of the C-scan along the y axis.

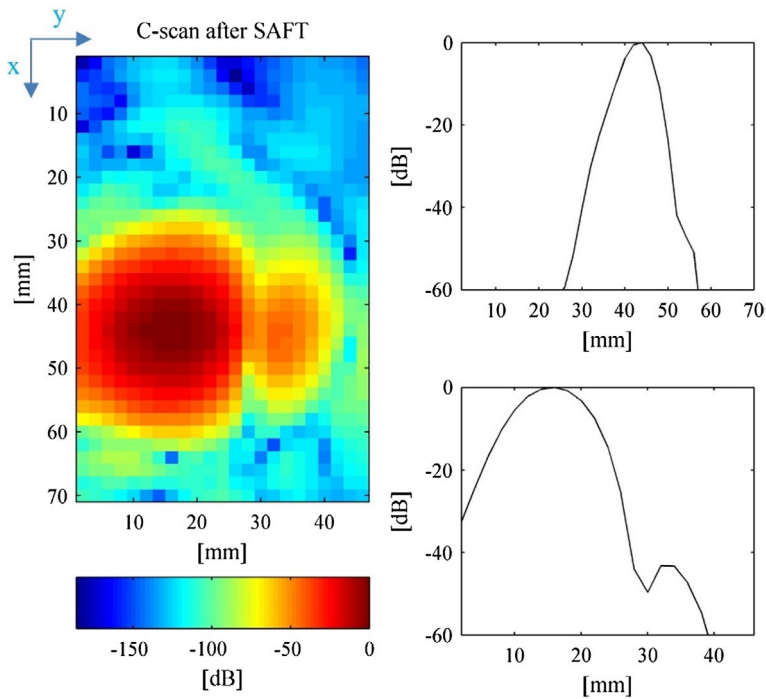


Figure 20. Analysis of the spatial resolution on SAFT data. (left) C-scan at $z = 80$ mm, (top right) cross-section of the C-scan along the x axis, (bottom right) cross-section of the C-scan along the y axis.

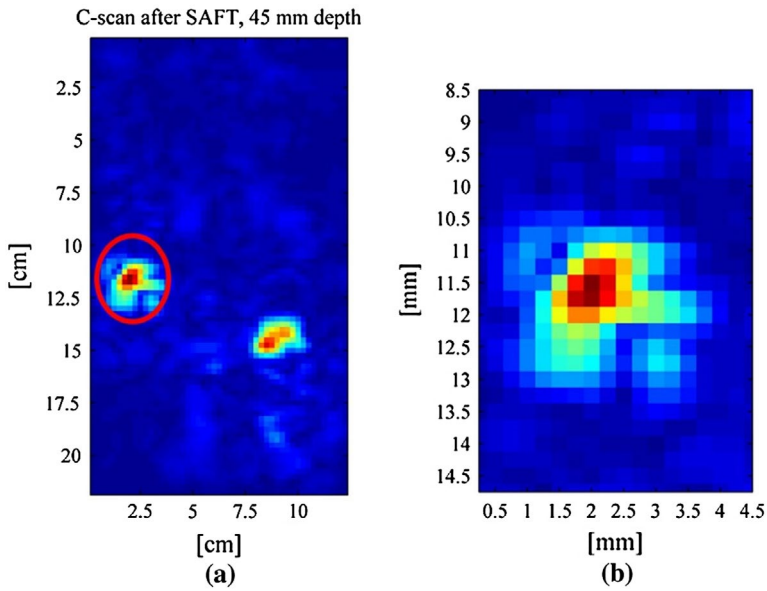


Figure 21. (a) SAFT image of the two bubble defects at a depth of 45 mm and (b) Enlarged view of the larger defect (circled).

Both the C-scan and SAFT images show clearly the presence of a defect. However, it is evident that the SAFT approach assures a better spatial resolution and a higher SNR. The gain in the resolution can be clearly appreciated by comparing Figures 19 and 20, which contain a cross-section through the drilled hole defect. The imaging capability of the standard C-scan relies on the availability of the acquired data for each-scanning point, as can be seen from Figure 19, where some data is missing or affected by lack of coupling. Conversely, the SAFT algorithm is robust against missing signals. That is because the SAFT algorithm combines signals collected in different scanning locations to obtain the correct signal amplitude at each scanning point.

Consider now the air bubble defects, which were at two slightly different depths into the polyurethane. Figure 21(a) shows the image obtained of the two air bubbles using the SAFT algorithm at a depth of 45 mm. Also, Figure 21(b) show an enlarged view of the larger defect (circled). The dimensions of each bubble were estimated to be 7–8 and 6 mm and respectively in diameter, and these estimates agree well with the sizes estimated from the photograph shown earlier in Figure 2.

4. Conclusions

The results show that PuC can be used to investigate materials with high attenuation of ultrasonic signals. The present experiments looked at 15 cm thick polyurethane riser stiffener samples, where the use of conventional NDT at frequencies above 1 MHz was not possible. Chirp signals and bipolar Golay codes were used in conjunction with piezocomposite transducers at a centre frequency of 300 kHz, so that the PuC technique could be applied. It was shown that, by careful consideration of the transducer spatial sensitivity in pitch-catch mode, it was possible to reconstruct images of both natural bubble defects and

an artificial flat-bottomed hole. C-scan data was effective, but improvements in SNR were available using a SAFT algorithm, adjusted to only consider regions in the sample over which the transduction system was sufficiently sensitive. The result is a technique that could be applied widely for thick, attenuating media.

Acknowledgements

Thanks are also due to Dr. Tom Knox for supplying the riser stiffener samples.

Disclosure statement

No potential conflict of interest was reported by the authors.

Funding

This work was funded via a grant from the Engineering and Physical Sciences Research Council (EPSRC), UK [grant number EP/K031201/1].

References

- [1] Moghimirad E, Mahloojifar A, Mohammadzadeh B. Computational complexity reduction of synthetic-aperture focus in ultrasound imaging using frequency-domain reconstruction. *Ultrason. Imaging*. 2016;38:175–193.
- [2] Chang C, Chang Y, Shih R, et al. Ultrasonic synthetic aperture focusing technique with finite source element for focused transducers. *J. Test. Eval*. 2014;42:1–9.
- [3] Skjelvareid MH, Birkelund Y, Larsen Y. Synthetic aperture focusing of outwardly directed cylindrical ultrasound scans. *IEEE Trans. Ultrason. Ferroelectr. Freq. Control*. 2012;59:2460–2469.
- [4] Deng R, Davies P, Bajaj AK. Flexible polyurethane foam modelling and identification of viscoelastic parameters for automotive seating applications. *J. Sound Vibr*. 2003;262:391–417.
- [5] Grad S, Kupcsik L, Gorna K, et al. The use of biodegradable polyurethane scaffolds for cartilage tissue engineering: potential and limitations. *Biomaterials*. 2003;24:5163–5171.
- [6] Boet WJC, Out JMM. Analysis of a flexible-riser top connection with bend restrictor. *Offshore Technology Conference*; Houston, USA; 1990.
- [7] Demanze F, Hanonge D, Chalumeau A, et al. Fatigue life analysis of polyurethane bending stiffeners. *ASME 2005 24th international conference on offshore mechanics and arctic engineering*; American Society of Mechanical Engineers; Houston, USA; 2005.
- [8] Marinho MG, dos Santos JM, Carneval RDO. Integrity assessment and repair techniques of flexible risers. *Proceedings of 25th international conference on offshore mechanics and arctic engineering*; Hamburg, Germany; Vol. 4, Paper No. OMAE2006-92467, p. 253–260; 8 pages. doi:10.1115/OMAE2006-92467.
- [9] Felix-Henry A, Lembeye P. Flexible pipes in-service monitoring. *Proceedings of 23rd international conference on offshore mechanics and arctic engineering*; Vancouver, British Columbia, Canada; 2004. Paper OMAE2004-51348.
- [10] Jacques R, Clarke T, Morikawa S, et al. Monitoring the structural integrity of a flexible riser during dynamic loading with a combination of non-destructive testing methods. *NDT & E Int*. 2010;43:501–506.
- [11] Veith E, Bucherie C, Lechien JL, et al. Inspection of offshore flexible riser with electromagnetic and radiographic techniques. *Proceedings of 15th world conference on non-destructive testing*; Rome, Italy; 2000.

- [12] Bastianini F, Di Tommaso A, Pascale G. Ultrasonic non-destructive assessment of bonding defects in composite structural strengthenings. *Compos. Struct.* **2001**;53:463–467.
- [13] Wright WMD, Hutchins DA, Schindel DW. Ultrasonic evaluation of polymers and composites using air-coupled capacitance transducers. In: Thompson DO and Chimenti DE, editors. *Review of progress in quantitative nondestructive evaluation*, New York, CO: Plennun Press; **1995**. Vol. 14B, p. 1399–1406.
- [14] McKie ADW, Addison RC, Jr. Laser-based ultrasonic inspection of complexly contoured rocket engine components. In: Thompson DO and Chimenti DE, editor. *Review of progress in quantitative nondestructive evaluation*, New York (CO): Plennun Press; **1998**. Vol. 17, p. 595–602.
- [15] Rao NAHK. Investigation of a pulse compression technique for medical ultrasound: a simulation study. *Med. Biol. Eng. Comput.* **1994**;32:181–188.
- [16] Torok R, Seller R. Pulse compression in search radar. *Periodica Polytech. Ser. El. Eng.* **1998**;42:391–408.
- [17] Gan TH, Hutchins DA, Billson DR, et al. The use of broadband acoustic transducers and pulse compression techniques for air-couple ultrasonic imaging. *Ultrasonics.* **2000**;39:181–194.
- [18] Seberry JR, Wysocki BJ, Wysocki TA. *Advanced signal processing for communication systems*. London: Kluwer Academic; **2002**. p. 182–196.
- [19] White JDH, Challis RE. A Golay sequencer based NDT system for highly attenuating materials. In: *Non-Contacting and Remote NDT, IEE Colloquium on, IET*; **1992**. p. 7–1.
- [20] Challis RE, Ivchenko VG. Sub-threshold sampling in a correlation-based ultrasonic spectrometer. *Meas. Sci. Technol.* **2011**;22:22–33.
- [21] Garcia-Rodriguez M, Yañez Y, Garcia-Hernandez MJ, et al. Application of Golay codes to improve the dynamic range in ultrasonic Lamb waves air-coupled systems. *NDT & E Int.* **2010**;43:677–686.
- [22] Nowicki A, Klimonda Z, Lewandowski M., et al. Direct and post-compressed sound fields for different coded excitations- experimental results. In: Andre PM, editor. *Acoustical imaging*. Vol. 28. New York (NY): Springer; **2007**. p. 399–407.
- [23] Krautkrämer J. Determination of the size of defects by the ultrasonic impulse echo method. *Br. J. Appl. Phys.* **1959**;10:240–245.
- [24] Wolf E, Marchand EW. Comparison of the Kirchhoff and the Rayleigh–Sommerfeld theories of diffraction at an aperture. *J. Opt. Soc. Am.* **1964**;54:587–594.
- [25] Hutchins D, Burrascano P, Davis L, et al. Coded waveforms for optimised air-coupled ultrasonic nondestructive evaluation. *Ultrasonics.* **2014**;54:1745–1759.
- [26] Pallav P, Gan TH, Hutchins DA. Elliptical-Tukey chirp signal for high-resolution, air-coupled ultrasonic imaging. *IEEE Trans. Ultrason. Ferroelectr. Freq. Control.* **2007**;54:1530–1540.
- [27] Spies M, Rieder H. Synthetic aperture focusing of ultrasonic inspection data to enhance the probability of detection of defects in strongly attenuating materials. *NDT & E Int.* **2010**;43:425–431.
- [28] Masri W, Mina M, Udpa SS, et al. Synthetic aperture focusing techniques applied in the near field of a focused transducer. *Ultrasonics Symposium, 1995. Proceedings, 1995 IEEE*; Vol. 1. IEEE; **1995**. p. 240–245.
- [29] Rudin LI, Osher S, Fatemi E. Nonlinear total variation based noise removal algorithms. *Physica D.* **1992**;60:259–268.
- [30] Ricci M, Callegari S, Caporale S, et al. Exploiting non-linear chirp and sparse deconvolution to enhance the performance of pulse-compression ultrasonic NDT. *Ultrasonics Symposium (IUS), 2012 IEEE International; IEEE*; **2012**.